EnvironmentAsia

Adsorption of Copper (II) and Nickel (II) by Chemical Modified Magnetic Biochar Derived from *Eichhornia crassipes*

Chompoonut Chaiyaraksa[*], Watcharapol Boonyakiat, Wannisa Bukkontod and Wanvisa Ngakom

Department of Chemistry, Faculty of Science, King Mongkut's Institute of Technology Ladkrabang (KMITL), Bangkok 10520, Thailand

*Corresponding Author: kcchompoonut@gmail.com

Abstract

A heavy metal contamination problem in Thailand is an important issue that needs to be addressed urgently, particularly contaminated in water. Heavy metal contamination in water can spread to other environments faster. This research aims to apply chitosan-magnetic biochar synthesized from water hyacinth in order to solve the problem of copper and nickel contaminated in water. Data from SEM indicated that chitosan-magnetic biochar had a smoother surface and had smaller holes than the magnetic biochar. When tested with Autosorb-1, results indicated that the adsorbent with chitosan had a slightly lower porosity compared to without chitosan. Data from FTIR found evidence of chitosan on the adsorbent. According to the XRD study, peaks of iron oxide presented. The point of zero charges (pH_{PZC}) of chitosan-magnetic biochar was 7.03. The adsorption isotherms, kinetics, and thermodynamics were observed. The adsorption of both Cu and Ni followed Langmuir isotherm. The value of q_{max} for Cu was 38.4615 mg/g and for Ni was 0.4858 mg/g. The R^2 value of Dubinin-Radushkevich isotherm was also high. The E value of Cu and Ni was 0.316 kJ/mol and 1.8962 kJ/mol, respectively. The best-fitting kinetic model for Cu was the pseudo-second-order model and for Ni was the intra-particle diffusion. The adsorption was an endothermic process. The process was spontaneous at high temperatures and non-spontaneous at low temperatures.

Keywords: Adsorption; Chitosan; Magnetic biochar; Metal; Wastewater

1. Introduction

The industrial growth and economic development of the country creates a wide range of environmental pollution. Major pollutants found in the environment are heavy metals such as copper, nickel, lead, and chromium. Heavy metals are raw materials used in many industries such as mining, electroplating, printing, paints, fertilizers, plastics, and batteries (Carolina *et al.*, 2017). There are various methods to solve the problem of heavy metal contamination in the environment such as coagulation, membrane separation, electrochemical treatment, electrodialysis, ion exchange, photocatalysis, and oxidation (Ahmed *et al.*, 2016A: Nguyen *et al.*, 2013: Farooq *et al.*, 2010: Ihsanullah *et al.*, 2016: Patil *et al.*, 2016). Absorption is gaining more attention nowadays due to it is easy to operate and lowest cost (Ojedokun and Bello, 2016). Moreover, if using waste materials such as water

hyacinth as an absorbent material, this will help to reduce waste and to add value to the waste. Previously, researchers have experimented on the use of water hyacinth roots to absorb Pb. The absorption capacity (Q_m) was 16.4 mg/g (Ye *et al.*, 2017). The powder of water hyacinth shoot had been made and packed in columns to treat wastewater containing Cr and Cu. It could remove ninety-nine percentage of metals (Hosseini *et al.*, 2016). The determination of the adsorption capacity of rice husk, palm leaf, and water hyacinth was on the ion of Cu, Co, and Fe. The adsorption capacity of water hyacinth was lowest (Tran *et al.*, 2017). Some researchers have conducted experiments by passing natural materials through a pyrolysis process and using them as an adsorbent. Results showed that the metal ion adsorption efficiency was better (Anzeze *et al.*, 2014). A pyrolysis temperature was also a factor effect on the metal ion adsorption efficiency (Sarkar *et al.*, 2017: Sadeek *et al.*, 2015: Cheng *et al.*, 2016). Biomass has been developed using several processes, such as activation by steam, acid solutions, basic solutions, and salts (Ahmed *et al.*, 2016B). Recently researchers interested in making the magnetic biochar to treat wastewater contaminated with cadmium (Zhang *et al.*, 2015). There are several ways to obtain such adsorbent. Each method produces an absorbent at different adsorption capacity (Mehta *et al.*, 2015). However, the research on this subject is still limited. This research thus aims to add value and benefit to water hyacinth by converting it to chitosan modified magnetic biochar and use it to solve the problem of copper and nickel contaminated wastewater.

2. Materials and Methods

2.1 Preparation of adsorbent (This method was modified from Cui *et al.*, 2016: Zheng *et al.*, 2016)

The absorbent preparation step was as follows: washed water hyacinth collected from Ladkrabang canal with water, cut into small pieces, dried at 100°C for 24 hours, let to cool at room temperature, crushed, sieved through a 35 mesh sieve, and divided the water

hyacinth powder into three parts. For the first part, making the biochar (B) was by passing the powder through the pyrolysis process at 400°C for 4 hours, washing with water to get rid of ash, and drying the solid residue at 100°C for 24 hours. For the second part, making the magnetic biochar (MB) was by immersing the powder in 2.5 M. FeCl$_3$ for 3 hours, heating the solution at 70°C for 0.5 hours, filtering, passing the powder through the pyrolysis at 400°C for 4 hours, washing with water to get rid of ash, and drying the solid residue at 100°C for 24 hours. For the last part, making the chitosan magnetic biochar (CMB) was firstly by doing the same process as the second part. The further process was as follows: immersing the powder in a chitosan solution (6 g chitosan dissolved in 1 L 2% acetic acid; v/v), shaking the solution at 40°C for 30 minutes, adding of 1 M NaOH to pH 9, further shaking at 40°C for 1 hour, filtering, and drying the solid residue at 100°C for 24 hours.

2.2 Synthetic wastewater preparation

Chemicals used to prepare the 1,000 mg/L of heavy metal ions stock solution were copper (II) sulfate pentahydrate and nickel (II) sulfate hexahydrate. A double distilled water was applied to dilute the stock solution to all desired metal concentrations. Preserving of the solution was by keeping in a refrigerator (4°C) under acid condition (pH < 2). All used chemicals were AR grade.

2.3 Adsorbent Characterization

Physical characteristic analyzation of biochar, magnetic biochar, and chitosan magnetic biochar was using scanning electron microscope (SEM) model 1455 VP (Leo), Fourier transform infrared spectrometer (FTIR) model Spectrum GX (Perkin Elmer), and X-ray diffractometer (XRD). Determination of the value of zero point charge was by pH drift method (Ahmed *et al.*, 2016).

2.4 Adsorption experiments

The 500 mL of synthetic wastewater with initial metal ion concentrations as required (C_0) was adjusted the pH to the desired value.

Table 1. Isotherm, kinetic, and thermodynamic equation

Isotherm	Linear equation
Langmuir	$\dfrac{C_e}{q_e} = \dfrac{C_e}{q_m} + \dfrac{1}{K_L.q_m}$ $R_L = \dfrac{1}{1+K_L.C_0}$
Freundlich	$log\ q_e = logK_f + \dfrac{1}{n}logC_e$
Tempkin	$q_e = \dfrac{RT}{b_0}lnA + \dfrac{RT}{b_0}lnC_e$
Dubinin-Radushkevich	$lnq_e = lnq_D - K_{DR}\left[RT\ ln\left(1+\dfrac{1}{C_e}\right)\right]^2$ $E = \dfrac{1}{\sqrt{2K_{DR}}}$
Kinetic	**Linear equation**
The pseudo-first order	$log(q_e - q_t) = logq_e - k_1\dfrac{t}{2.303}$
The pseudo-second order	$\dfrac{1}{q_t} = \dfrac{1}{k_2q_e^2} + \dfrac{t}{q_e}$
Elovich	$q_t = \dfrac{1}{\beta}ln(\alpha\beta) + \dfrac{1}{\beta}ln\ t$
The intraparticle diffusion	$q_t = K_{id}(t)^{\frac{1}{2}} + C$
Thermodynamic	**Equation**
	$\Delta G^0 = \Delta H^0 - T\Delta S^0$ $\Delta G^0 = -RT\ lnK_c$ $K_c = \dfrac{q_e}{C_e}$ $lnK_c = \dfrac{\Delta S^0}{R} - \dfrac{\Delta H^0}{RT}$

q_t = the amount of adsorbed metal per unit mass of adsorbent at time t (mg/g)
q_e = the amount of adsorbed metal per unit mass of adsorbent at equilibrium (mg/g)
C_t, C_0, C_e = the metal concentration in solution at time t, 0, and equilibrium, respectively (mg/L)
V = the volume of the solution (L)
W = the mass of dry adsorbent (g)
q_m = the maximum adsorbed metal amount per unit mass of sorbent (mg/g)
K_L = Langmuir constant (L/mg)
R_L= a dimensionless separation factor or equilibrium parameter
K_f= Freundlich constant (L/g)
$1/n$ = the value related to the adsorption intensity
A = Temkin isotherm constant (L/g) corresponding to the maximum binding energy
b_0 = Temkin constant related to heat of sorption (J/mol)
R = the gas constant (8.314 J/mol.K)
T = the absolute temperature (K)
q_D = the adsorption capacity (mg/g)
K_{DR} = the constant (mol²/kJ²)
E = the mean adsorption energy (kJ/mol) of the adsorbate
k_1 = the rate constant for pseudo-first order adsorption (1/min).
k_2 = the rate constant for pseudo-second order adsorption (g/mg.min)
α = the initial adsorption rate (mg/g min)
β = the constant related to the extent of surface coverage and the activation energy for chemisorptions (g/mg).
K_{id} = the intraparticle diffusion rate constant (mg/g min$^{1/2}$)
K_c = the equilibrium constant reflected the adsorbent ability to keep the adsorbate and extent the adsorbate movement within the solution.

Adding the required amount of an adsorbent (m) to the solution, shaking of the solution at a speed of 800 rpm over a specified period (t) and temperature (T) and then filtering under pressure were performed. Determination of the metal concentration in the aliquot was by Atomic absorption spectrometer (AAS) model AAnalyst 200, Perkin Elmer. The factors influencing the adsorption were varied as follows: pH 2-8, m 25-200 mg, C_0 25-300 mg/L and T 35°-55°C.

2.5 Study of Isotherm, kinetic, and thermodynamic
    The consideration was on four different isotherms and kinetics as in Table 1 (Han *et al.*,

2016: Shang *et al.*, 2016). The evaluation was also on changing of free energy (ΔG˚), enthalpy (ΔH˚) and entropy (ΔS˚) (Razvigorova *et al.*, 1998).

$$q_t = \frac{(C_0 - C_t)}{W}x\ V$$

$$q_e = \frac{(C_0 - C_e)}{W}x\ V$$

$$\%\ removal = \frac{(C_0 - C_e)}{C_0}x100$$

3. Results and discussion

3.1 Adsorbent Characterization

The FTIR spectra in Figure 1 (B) showed the band at 3,420.81 cm^{-1} (O-H and N-H), 2,924.13 cm^{-1} (C-H), 1601.91 cm^{-1} (-C=O), and 1425.42 cm^{-1} (O-H) which indicating of the presenting of cellulose and hemicellulose due to a low pyrolysis temperature. Figure 1 (MB) and (CMB) showed the evidence of Fe–O bonds at about 556.47 cm^{-1} and Figure 1 (CMB) also had the evidence of chitosan. The dominant band was at 1,261 cm^{-1} (C-N), 1,095 cm^{-1} and 1031 cm^{-1} (C=O).

Figure 2 showed the SEM image of adsorbents. The surface of the biochar (B) was smoothest comparing to the others. There was more porosity in the surface of the magnetic biochar (MB) than the biochar. The rougher surface presented for the magnetic biochar (MB) due to the iron oxide deposition on the surface. The chitosan coating the pore surface of the modified magnetic biochar (CMB) resulted in a smoother surface around those pores.

XRD pattern in Figure 3 (b) and (c) shows peaks of iron oxide at 2-theta 33.5°, 35.6°, 41.89.5°, and 62.8°.

Figure 4 showed the relationship between initial acidity (pH$_i$) and final pH (pH$_f$). The point of zero charge (pH$_{PZC}$) of chitosan magnetic biochar was 7.03. When this adsorbent was in a solution with a higher pH, the surface of
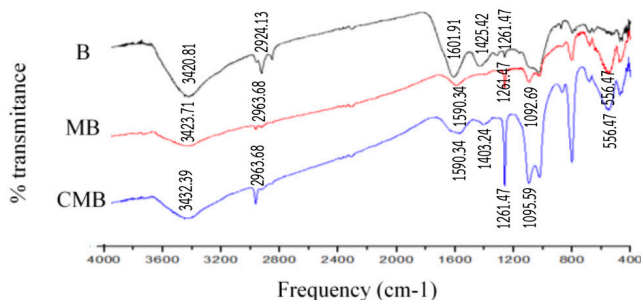

Figure 1. FTIR spectra of biochar (B), magnetic biochar (MB), chitosan magnetic biochar (CMB)
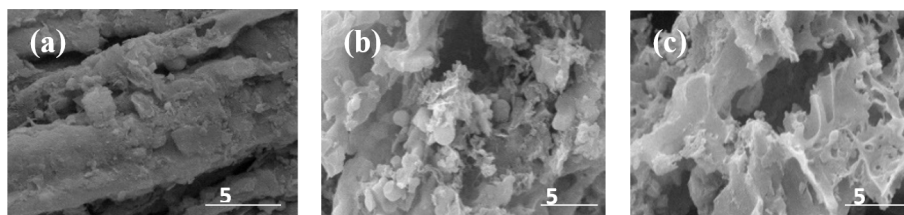

Figure 2. SEM image of a) biochar b) magnetic biochar c) chitosan magnetic biochar
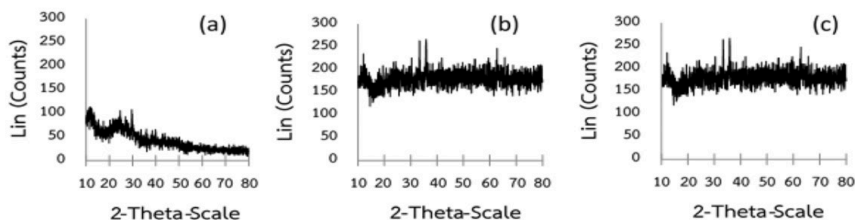

Figure 3. XRD pattern of a) biochar b) magnetic biochar c) chitosan magnetic biochar
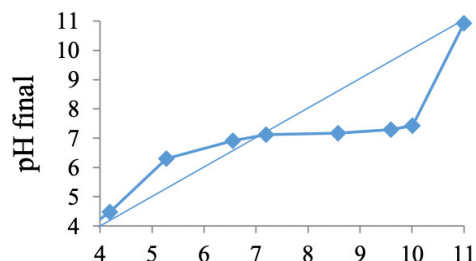
Figure 4. Point of zero charge (pH_{PZC}) of chitosan magnetic biochar
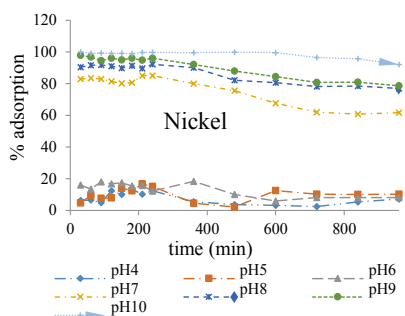

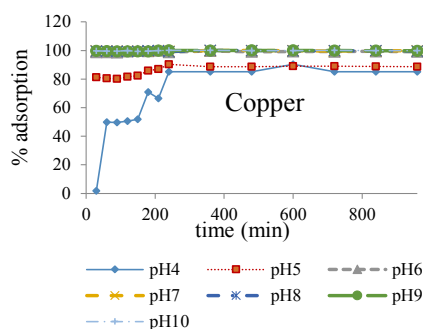**Figure 5.** Ni removal percentage when the initial solution pH 4-10.

Figure 6. Cu removal percentage when the initial solution pH 4-10.

the adsorbent was negative charges and, in the opposite direction, the surface the adsorbent was positive charges when it was in a solution with a lower pH.

3.2 Effect of pH and reaction time on adsorption by MBC

Preparing the solution with different pH values ranging from 4.0 to 10.0 and testing the adsorption capacity of MBC, results were as in Figure 5 and 6. The percentage of Ni removal was very low at the initial solution pH 4-6 and significantly increased at the initial solution pH

7-10 (Figure 5). The Cu adsorption capacity was higher than the adsorption capacity of Ni, especially at pH 6-10 (Figure 6). The point of zero charge of MBC was 7.03. The metal ion adsorption was decreased with the lessening of pH as a possible result of the positive charges of the adsorbent surface repelling metal ions (Shamel *et al.*, 2016). With too high pH solution (pH > 8), copper and nickel precipitation would occur thus selecting pH 7 for further experiments. From Figure 5 and 6, the 30 minutes shaking time was enough to reach the adsorption equilibrium.

Table 2. Isotherm parameters of Cu and Ni

Cu		Ni	
Langmuir isotherm		**Langmuir isotherm**	
q_{max} (mg/g)	38.46	q_{max} (mg/g)	0.48
K_L (L/mg)	0.33	K_L (L/mg)	0.01
R_L	0.06	R_L	0.93
R^2	1	R^2	1
Freundlich isotherm		**Freundlich isotherm**	
K_F (L/mg)	23.67	K_F (L/mg)	3.16
1/n	0.11	1/n	-92.24
R^2	0.9775	R^2	0.9163
Dubinin-Radushkevich isotherm		**Dubinin-Radushkevich isotherm**	
K_{Dr}	2.00	K_{Dr}	0.14
q_D (mg/g)	36.28	q_D (mg/g)	3.33
E (kJ/mol)	0.31	E (kJ/mol)	1.89
R^2	0.9955	R^2	0.9198
Temkin isotherm		**Temkin isotherm**	
b_o (kJ/mol)	0.28	b_o (kJ/mol)	50423
A (L/mg)	11.35	A (L/mg)	-
R^2	0.9812	R^2	0.756

3.3 Adsorption isotherm study

The adsorption of 160 mg/L heavy metal ions was carried out using 25, 100, and 150 mg. of CMB. The experimental results were calculated using the adsorption isotherm of Langmuir, Freundlich, Temkin, and Dubinin-Radushkevich. The calculation results were as in Table 1.

Four isotherms were applied to fit with the experimental data giving the correlation values that lied between 0.7560 and 1. The best-fitting and the most applicable use of the isotherms were Langmuir with the R^2 value of 1. This adsorption model assumes that each molecule of adsorbent absorbs only one molecule of an adsorbate. The adsorbed molecules that are in close to one another do not have a force between themselves, or they do not react to each other. The adsorbed molecules cannot be displaced. The molecules of the adsorbed material are of a certain number. The adsorption take place in a certain position. The heat of adsorption is equal and constant in all adsorption position.

The value of q_{max} was 38.46 mg/g for Cu and 0.48 mg/g for Ni. The value of R_L ($0 > R_L < 1$) indicated that the adsorption fits with Langmuir isotherm. The R^2 value of Dubinin-Radushkevich isotherm was also high. The mean adsorption energy of the CMB was less than 8 kJ/mol; this indicated the naturally physical in the adsorption process. Inengite *et al.* (2014) reported the similar results to this study. The value of E in Dubinin-Radushkevich isotherm was 0.35. When considering Temkin isotherm of copper adsorption, the correlation coefficient (R^2) was 0.9812. The b_0 value of copper adsorption was 0.28 kJ/mol. The result indicated that the main adsorption mechanism was the physical process. While the correlation coefficient (R^2) of nickel adsorption was low, Temkin was inappropriate to describe the isotherm.

3.4 Kinetic study

The adsorption of Cu and Ni ions by CMB was carried out by varying the initial

Table 3. Kinetic parameters for Cu adsorption by CMB

Copper	Initial concentration (mg/L)			System temperature (˚C)		
	120	160	200	35	45	55
Pseudo-first-order						
k_1 (1/min)	0.0143	0.0088	0.0096	0.0161	0.0121	0.0217
q_e (mg/g)	20.6918	20.6585	33.9078	70.3720	57.5439	58.2371
R^2	0.7493	0.6135	0.8594	0.8746	0.9717	0.9965
Pseudo-second-order						
k_2 (g/mg min)	0.0189	0.0193	0.0284	0.0057	0.0059	0.0067
q_e (mg/g)	40.1606	57.1428	75.1879	57.5193	62.8930	68.4931
R^2	0.9969	0.9998	0.9992	0.9964	0.9667	0.9880
Elovich						
α (mg/g min)	69.2871	368.5286	379.2732	20.5314	20.5654	99.4094
β (mg/g)	0.0957	0.0678	0.0516	0.0516	0.0649	0.0568
R^2	0.9018	0.8719	0.9493	0.9617	0.9869	0.9539
Intra-particle diffusion						
K_{id} (mg/g min)	5.5739	7.6866	10.187	10.4369	8.5631	9.4471
R^2	0.7845	0.7456	0.8501	0.8704	0.9598	0.8712

Table 4. Kinetic parameters for Ni adsorption by CMB

Nickel	Initial concentration (mg/L)			System temperature (oC)		
	120	160	200	35	45	55
Pseudo-first order						
k_1 (1/min)	0.0094	0.0085	0.0044	0.0052	0.0057	0.0069
q_e (mg/g)	97.1628	73.097	95.9842	95.8296	159.0011	115.0006
R^2	0.9091	0.893	0.9505	0.9716	0.8623	0.9332
Pseudo-second order						
k_2 (g/mg min)	0.0005	0.0025	0.0003	0.0005	-0.0377	0.0003
q_e (mg/g)	94.3396	72.4637	83.3333	80.6451	32.8947	126.5823
R^2	0.642	0.941	0.459	0.4307	0.2925	0.6487
Elovich						
α (mg/g min)	449.3394	655.9337	562.5252	411.7742	19.3168	921.4248
β (mg/g)	0.0543	0.0584	0.0710	0.0640	0.0235	0.0446
R^2	0.8828	0.9748	0.7896	0.8523	0.8358	0.8708
Intra-particle diffusion						
K_{id} (mg/g min)	8.5153	9.5877	10.797	9.2155	12.85	13.069
R^2	0.9534	0.9607	0.9085	0.9134	0.8627	0.9541

Table 5. Thermodynamic parameters for Cu and Ni adsorption by CMB

	ΔH° (kJ/mol)	ΔS° (J/mol.K)	ΔG° (kJ/mol)		
			35˚C	45˚C	55˚C
Cu	30.8034	116.1549	-5.0036	-6.1656	-7.3276
Ni	23.8329	72.3334	1.1008	0.3778	-0.3452

concentration of heavy metal ions and system temperature. The experimental results were calculated using four adsorption kinetic equations. The calculation results were as in table 3 and table 4.

The author used four kinetic models to fit experimental data. The correlation value was between 0.6135 and 0.9998. From Table 3, the most applicable use of the kinetic model with the best-fitting for Cu was the pseudo-second-order kinetic with the R^2 value of 0.9667-0.9998. The indicating of the best fit of the pseudo-second-order kinetic was the interaction forming between adsorbate and adsorbent on the external surface. The work of Shang *et al.* (2016) on Cr adsorption onto magnetic biochar from Astragalus mongholicus had concluded that the pseudo-second-order kinetic was the best model for adsorption kinetic describing. The pseudo-second-order kinetic data also indicated the higher the initial Cu ion concentration and system temperature led to the higher the k_2 and q_e. The Elovich plot at various initial Cu ion concentrations and system temperatures were linearly in the good correlation coefficient ($R^2 = 0.8719$ to 0.9869). The initial adsorption rate, α, increased while the initial Cu ion concentration increased. The Elovich model was better describing the adsorption kinetics of an ion exchanging system. Normally, the equation was valid for the systems in which the adsorbing surface was heterogeneous (Li *et al.*, 2015).

From Table 4, the most applicable use of the kinetic model with best-fitting was intra-particle diffusion. The intraparticle diffusion rate constant (K_{id}) increased as the concentration of nickel in synthetic wastewater increased. When increasing the temperature, the intraparticle diffusion rate constant increased as the higher the temperature, the less air inside

the pores. Copper ions could move inside the pore easier.

3.5 Thermodynamic study

Table 5 showed thermodynamic parameters. The negative value of ΔG° indicated the occurring of the natural adsorption. The value of ΔG° was slightly lessening with the increase in temperature. It was an indication of the endothermic adsorption process.

In general, the change in adsorption enthalpy for physisorption ranged from -20 to 40 kJ/mol while the chemisorption was between -400 and -80 kJ/mol. The value of ΔH° for Cu and Ni revealed the physisorption adsorption in nature. When $\Delta S > 0$ and $\Delta H > 0$, the process was spontaneous at high temperatures and non-spontaneous at low temperatures.

4. Conclusions

The confirmation by this study was that the prepared chitosan magnetic biochar by water hyacinth with the low cost and easily available at the environmentally problematic plant could effectively remove copper from wastewater. However, the adsorbent needed to be improved to solve the problem of Ni contaminated in wastewater.

Acknowledgments

References

Ahmed MB, Zhou JL, Ngo HH, Guo W, Chen M. Progress in the preparation

and application of modified biochar for improved contaminant removal from water and wastewater. Bioresource Technology 2016B; 214: 836–851.

Ahmed MJK, Ahmaruzzaman M. A review on potential usage of industrial waste materials for binding heavy metal ions from aqueous solutions. Journal of Water Process Engineering 2016A; 10: 39–47.

Anzeze DA, Onyari JM, Shiundu PM, Gichuki JW. Adsorption of Pb (II) ions from aqueous solutions by water hyacinth (*Eichhornia Crassipes*): Equilibrium and kinetic studies. International Journal of Environmental Pollution and Remediation 2014; 2: 89-95.

Carolina CF, Kumara PS, Saravanana A, Joshibaa GJ, Naushadb M. Efficient techniques for the removal of toxic heavy metals from aquatic environment: A review. Journal of Environmental Chemical Engineering 2017; 5: 2782–2799.

Cheng Q, Huang Q, Khan S, Liu Y, Liao Z, Li G, Ok YS. Adsorption of Cd by peanut husks and peanut husk biochar from aqueous solutions. Ecological Engineering 2016; 87: 240–245.

Cui X, Fang S, Yao Y, Li T, Ni Q, Yang X, He Z. Potential mechanisms of cadmium removal from aqueous solution by Canna indica derived biochar. Science of the Total Environment 2016; 562: 517–525.

Farooq U, Kozinski JA, Khan MA, Athar M. Biosorption of heavy metal ions using wheat based biosorbents – A review of the recent literature. Bioresource Technology 2010; 101: 5043–5053.

Han Y, Cao X, Ouyang X, Sohi SP, Chen J. Adsorption kinetics of magnetic biochar derived from peanut hull on removal of Cr (VI) from aqueous solution: Effects of production conditions and particle size. Chemosphere 2016; 145: 336-341.

Hosseini SS, Bringas E, Tan NR, Ortiz I, Ghahramani M, Shahmirzadi MAA. Recent progress in development of high performance polymeric membranes and materials for metal plating wastewater treatment: A review. Journal of Water Process Engineering 2016; 9: 78-110.

Ihsanullah, Abbas A, Al-Amer AM, Laoui T, Al-Marri MJ, Nasser MS, Khraisheh M, Atieh MA. Heavy metal removal from aqueous solution by advanced carbon nanotubes: critical review of adsorption applications. Separation and Purification Technology 2016; 157: 141–161.

Inengite AK, Abasi CY, Johnny DB. Equilibrium studies of methylene blue dye sorption by dried water hyacinth shoot. Environment and Natural Resources Research 2014; 4(4):120-129.

Li F, Shen K, Long X, Wen J, Xie X, Zeng X, Liang Y, Wei Y, Lin Z, Huang W, Zhong R. Preparation and characterization of biochars from Eichornia crassipes for cadmium removal in aqueous solutions. Plos One 2015; 11(2): 1-13.

Mehta D, Mazumdar S, Singh SK. Magnetic adsorbents for the treatment of water/wastewater—A review. Journal of Water Process Engineering 2015; 7: 244–265.

Nguyen TAH, Ngo HH, Guo WS, Zhang J, Liang S, Yue QY, Li Q, Nguyen TV. Applicability of agricultural waste and by-products for adsorptive removal of heavy metals from wastewater. Bioresource Technology 2013; 148: 574–585.

Ojedokun AT, Bello OS. Sequestering heavy metals from wastewater using cow dung. Water Resource and Industry 2016; 13: 7–13.

Patil DS, Chavan SM, Oubagaranadin JUK. A review of technologies for manganese removal from wastewaters. Journal of Environment Chemical Engineering 2016; 4: 468–487.

Razvigorova M, Budinova T, Petrov N, Minkova V. Purification of water by activated carbons from apricot stones, lignites and anthracite. Water Research 1998; 32(7): 2135–2139.

Sadeek SA, Negm NA, Hefni HHH, Wahab MMA. Metal adsorption by agricultural biosorbents: Adsorption isotherm, kinetic and biosorbents chemical structures. International Journal of Biological Macromolecules 2015; 81: 400–409.

Sarkar M, Rahman AKML, Bhoumik NC. Remediation of chromium and copper on water hyacinth (E. crassipes) shoot powder. Water Resources and Industry 2017; 17: 1–6.

Shamel A, Khoshraftar Z, Alayi R. Adsorption of cationic dye from aqueous solution onto sea shell as an adsorbent low-cost: Kinetic studies. Der Pharma Chemica 2016; 8(5): 60-66.

Shang J, Pi J, Zong M, Wang Y, Li W, Liao Q. Chromium removal using magnetic biochar derived from herb-residue. Journal of the Taiwan Institute of Chemical Engineers 2016; 68: 289–294.

Tran TK, Chiu KF, Lin CY, Leu HJ. Electrochemical treatment of wastewater: Selectivity of the heavy metals removal process. International Journal of Hydrogen Energy 2017; 42(45): 27741-27748.

Ye M, Li G, Yan P, Ren J, Zheng L, Han D, Sun S, Huang S, Zhong Y. Removal of metals from lead-zinc mine tailings using bioleaching and followed by sulfide precipitation. Chemosphere 2017; 185: 1189-1196.

Zhang F, Wang X, Yin D, Peng B, Tan C, Liu Y, Tan X, Wu S. Efficiency and mechanisms of Cd removal from aqueous solution by biochar derived from water hyacinth (Eichornia crassipes). Journal of Environmental Management 2015; 153: 68–73.

Zheng J, Liu H, Feng H, Li W, Lam MH, Lam PK, Yu H. Competitive sorption of heavy metals by water hyacinth roots. Environmental Pollution 2016; 219: 837–845.